covSTATIS: a multi-table technique
for network neuroscience

Giulia Baracchini[1*], Ju-Chi Yu[2*], Jenny Rieck[3], Derek Beaton[4], Vincent Guillemot[5], Cheryl Grady[3,6], Hervé Abdi[7], R. Nathan Spreng[1]

Affiliations

[1] Montreal Neurological Institute, Department of Neurology and Neurosurgery, McGill University, Montreal, Canada
[2] Campbell Family Mental Health Institute, Centre for Addiction and Mental Health, Toronto, Canada
[3] Rotman Research Institute at Baycrest, Toronto, Canada
[4] Data Science & Advanced Analytics, Unity Health Toronto, Toronto, Canada
[5] Institut Pasteur, Université Paris Cité, Bioinformatics and Biostatistics Hub, Paris, France
[6] Departments of Psychiatry and Psychology, University of Toronto, Toronto, Canada
[7] School of Behavioral and Brain Sciences, The University of Texas at Dallas, Richardson, USA

*These authors contributed equally to this work

Correspondence

Giulia Baracchini: giulia.baracchini@mail.mcgill.ca

Abstract

Similarity analyses between multiple correlation or covariance tables constitute the cornerstone of network neuroscience. Here, we introduce covSTATIS, a versatile, linear, unsupervised multi-table method designed to identify structured patterns in multi-table data, and allow for the simultaneous extraction and interpretation of both individual and group-level features. With covSTATIS, multiple similarity tables can now be easily integrated, without requiring *a priori* data simplification, complex black-box implementations, user-dependent specifications, or supervised frameworks. Applications of covSTATIS, a tutorial with Open Data and source code are provided. CovSTATIS offers a promising avenue for advancing the theoretical and analytic landscape of network neuroscience.

Main

Correlation, covariance and distance matrices are among the most commonly used data types in network neuroscience[1–4]. They are typically built via pairwise comparisons of functional and/or structural neuroimaging data. In these matrices, one entry stores a numerical value quantifying the similarity between two spatial locations (i.e., brain voxels, vertices, regions, channels) and the pattern of these entries reflects an estimate of brain network organization.

In network neuroscience, matrices—also called here data tables—are typically obtained from sets of variables collected on the same individuals (e.g., multiple scans or sessions, multiple imaging modalities)[5–9], or from the same variables collected on different individuals (e.g., one type of imaging scan on several participants)[10–13]. Data tables are then compared to one another to assess temporal network structure[14–17], multi-modal network organization[4,18,19], individual differences[20–25], and group or population effects[26–30]. Data tables are also contrasted with one another to investigate the statistical reliability of patterns derived from network neuroscience methods[31,32]. Similarity analyses among multiple data tables thus constitute the cornerstone of network neuroscience research.

In network neuroscience, similarity analyses are most often conducted on aggregate information within data tables (e.g., graph theory analyses[33]) or across (e.g., categorical groupings), or on single tables with reduced dimensions (e.g.,[34]). While these approaches reduce the high dimensionality of network neuroscience data and simplify the analytic landscape, they may obscure important properties of brain function that could be revealed from the analysis of full data tables. Approaches able to align and compare relational information from full data tables across multiple observations, can augment the utility, precision, and applicability of network neuroscience data and advance our understanding of brain network organization in health and disease.

Statistical methods exist— called multi-table methods[35–43]—explicitly designed for similarity analyses of full data tables. Their goal is to identify structured patterns within preserved high-dimensional multi-table data and explain and visualize their statistical dependencies. Multi-table methods serve as the basis of network investigations across scientific disciplines (e.g.,[44]), yet they are not well known in network neuroscience and therefore remain underused.

Network neuroscience presently counts a few multi-table methods, including machine learning and deep learning tools[45,46], graph neural networks[47,48], multi-layer and multiplex networks approaches[18,49], similarity network fusion techniques[50] and non-linear matrix decomposition algorithms[51–53]. These approaches have been applied to a variety of research questions about brain

network organization both in health and disease[54–61]. Yet, they often yield complex results challenging to interpret, potentially because these methods rely on complex mathematical implementations[62,63] and supervised analytical frameworks[51] that do not allow results to be traced back to the original data. There is therefore a pressing need in network neuroscience for multi-table methods that preserve data fidelity and enhance interpretability. CovSTATIS solves this problem by analyzing intact data tables in a linear, unsupervised manner, thus allowing for the simultaneous extraction and interpretation of both individual and group-level features.

The covSTATIS method (and its variant DISTATIS) first appeared in[64] and is a three-way extension of multidimensional scaling and Principal Component Analysis[64–66]. The name, covSTATIS, combines "covariance" with "STATIS" (a French acronym for "structuring three-way statistical tables"). CovSTATIS takes as input symmetric, positive semi-definite matrices (i.e. symmetric matrices such as cross-product, covariance and correlation matrices) and assesses their similarity[67–69]. While covSTATIS is specifically designed for correlation/covariance matrices, there exists an equivalent approach for distance matrices called DISTATIS[64]. CovSTATIS and DISTATIS belong to the STATIS family of multi-table approaches. In neuroimaging, STATIS-based techniques have been applied in a limited capacity[70–76]. In network neuroscience, recent work from our group applied covSTATIS to compare spatial patterns of fMRI connectivity across task states[77], and to estimate resting-state fMRI connectivity dynamics[78].

In covSTATIS, the similarity among multiple correlation/covariance matrices is quantified by the R_V coefficient—a matrix analogous to a squared correlation coefficient—which takes values in the interval $[0,1]$[67,79]. These coefficients are stored in an R_V *similarity matrix* where each row/column corresponds to a single data table (**Figure 1, step 1**). Next, covSTATIS performs an eigenvalue decomposition (EVD) on the R_V similarity matrix and takes the resulting first eigenvector to derive weights for each data table. Note that because the R_V is always positive, all the entries for the first eigenvector are positive—a property derived from the Perron-Frobenius theorem. The first eigenvector maximally explains the variance in the R_V matrix and quantifies how similar each table is to the common pattern. Weights for each data table are derived by scaling the first eigenvector to sum to 1. Higher weights identify tables that are more similar to the common pattern, whereas lower weights identify tables less similar to the common pattern. These weights are then used to linearly combine the data tables by multiplying each table by its weight and summing across all the weighted tables. This step generates a weighted group matrix—called the *compromise matrix* (**Figure 1, step 2**)—which is next decomposed by EVD. Orthogonal components are extracted from this second EVD and serve as the main output of covSTATIS (**Figure 1, step 3**).

Components reveal the similarity between variables with regards to the compromise—the ensemble of the similarity patterns across all data tables. For each component, *factor scores* are used to reconstruct and interpret covSTATIS' output in relation to the original data, yielding 1) *global factor scores* that represent associations between variables with respect to the compromise, and 2) *partial factor scores* that represent associations within each data table separately (**Figure 1, step 4**). For example, given a covSTATIS analysis of multiple functional connectivity matrices where only positive connectivity values are considered, *global factor scores* represent the brain regions on the component space and illustrate the associations in their connectivity profiles across the whole sample. *Partial factor scores* represent the brain regions of each individual's connectivity matrix and illustrate how regions are associated with each other in relation to the group pattern. Factor scores of any two components can be used as coordinates to draw scatter plots in the component space, where the distance between two scores represents their similarity. Two *global factor scores* close to each other indicate high similarity in their respective connectivity patterns across the whole sample, while a *partial factor score* close to its corresponding global factor score represents high similarity between an individual's regional connectivity profile and the regional profile from the whole sample. In sum, covSTATIS provides an unsupervised, linear framework to characterize the similarity among sets of correlation/covariance matrices, and it allows for a one-to-one mapping between input (i.e., whole set of tables and single tables) and output (i.e., *global* and *partial factor scores*). This approach can both identify group-level patterns as well as provide individual-specific expressions of the patterns.

The potential of covSTATIS as a tool for network neuroscience remains largely untapped. Examples of potential applications of covSTATIS include investigations of individual and group differences in spatial and/or temporal network structure in health and disease (**Figure 2, bottom panel**), deep phenotyping of connectivity metrics, and multimodal assessments of network measures within and across individuals (**Figure 2, top panel**). With covSTATIS, multiple types of data tables can now be easily integrated, without requiring *a priori* data simplification, complex black-box implementations, user-dependent specifications or supervised theoretical frameworks. Another promising avenue for covSTATIS is the exploration of brain-behavior relationships within a single framework. Through covSTATIS, participants' correlations—computed from high dimensional brain and behavioral data tables—can be integrated in a unified compromise space from which the shared variance between tables can be extracted. While not exhaustive, the proposed applications of covSTATIS highlight the versatility of the method. We hope that the network neuroscience community will benefit from covSTATIS and collectively further refine and expand the approach. Ongoing developments of covSTATIS can be found on our website: https://giuliabaracc.github.io/covSTATIS_netneuro/.

To facilitate adoption of covSTATIS, we provide a step-by-step tutorial using Open Data[80]. In this tutorial, we use covSTATIS to examine how fMRI-derived functional connectivity reconfigures across task conditions with increasing cognitive load (0-back, 1-back, 2-back), in a healthy adult lifespan sample of 144 individuals. The tutorial can be accessed here: https://giuliabaracc.github.io/covSTATIS_netneuro/pages/tutorial.html. In the tutorial, we additionally guide the reader in the choice of covSTATIS' parameters based on the type of input data.

CovSTATIS serves as a theoretically and computationally accessible tool for similarity analyses, capable of preserving and integrating high dimensional, complex multi-table data typical of network neuroscience. Its linear, unsupervised, user-independent implementation makes covSTATIS a highly interpretable and versatile tool designed to pave the path for new discoveries in network neuroscience.

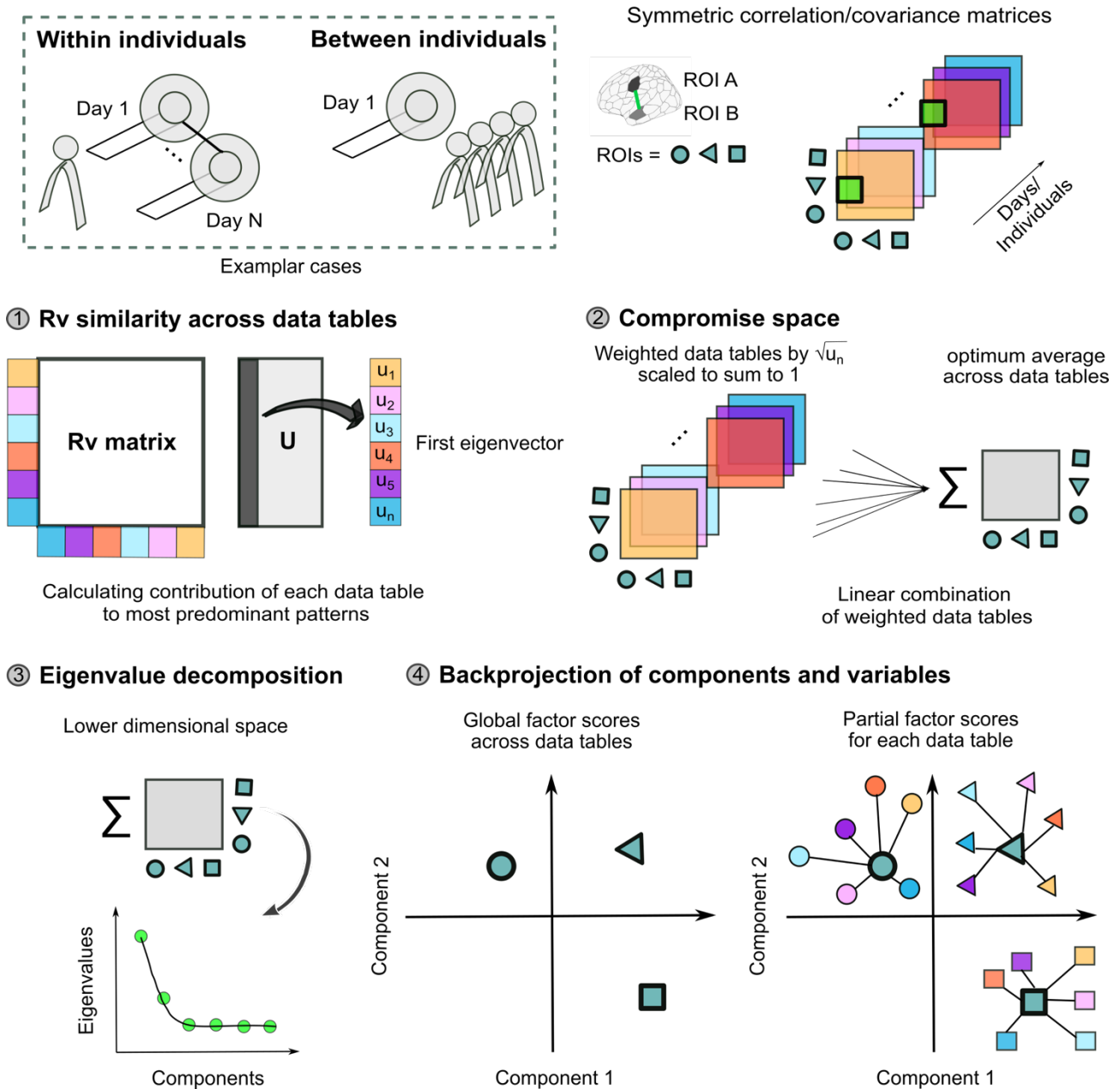# covSTATIS: a multi-table method for network neuroscience

Figure 1. CovSTATIS is used to analyze multiple correlation/covariance matrices obtained either within or between individuals. We provide an example using functional connectivity matrices, collected on multiple individuals, as input to covSTATIS. **(1)** First, covSTATIS combines all connectivity matrices by quantifying their overall similarity via their R_V coefficients. These coefficients are then stored in the $\mathbf{R_V}$ matrix. Next, covSTATIS uses the first eigenvector ($\mathbf{u}_1$) of the $\mathbf{R_V}$ matrix to derive weights for each connectivity matrix. **(2)** With these weights, covSTATIS computes the linear combination of all matrices to generate a common space, the *compromise*, which best represents the connectivity pattern across the sample. **(3)** The *compromise* then undergoes eigenvalue decomposition and orthogonal components are extracted to characterize the variance in the whole-sample connectivity pattern. **(4)** The variables of the compromise (illustrated by different shapes of green points; i.e., individual brain regions) are represented as *global factor scores* in the component space. *Global factor scores* represent the connectivity pattern of each brain region across the entire sample. The same variables from each individual matrix can also be back projected onto the same space as *partial factor scores* (indicated by points with the same shape of different colors). *Partial factor scores* represent the connectivity pattern of each brain region for a specific individual. Importantly, the weighted means of all partial factor scores of a given variable equal to their global factor scores (i.e., barycentric property). In this component space, the distance between factor scores provides meaningful and interpretable information about the similarity in the connectivity profile of any two brain regions. The closer the (global or partial) factor scores of two brain regions, the more similar their connectivity profiles.

# covSTATIS: examples of applications in network neuroscience

Type of research question	Global factor scores	Partial factor scores
Group comparison/ individual differences	Group means of ROIs/networks	ROI/network configuration per group or individual
Deep phenotyping	Session means of ROIs/networks	ROI/network configuration per session
Task/condition differences	Tasks/condition means of ROIs/networks	ROI/network configuration per task/condition
Multimodal neuroimaging	Modality means of ROI/networks	ROI/network configuration per neuroimaging modality
Temporal profiling of network structure (e.g., dynamic functional connectivity)	Means of time chunks (e.g., across sliding windows) of ROI/networks	ROI/network configuration per time chunk (e.g. per window)

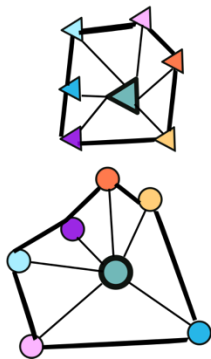① **Examples of extractable features**
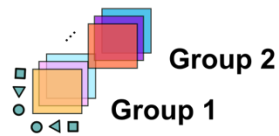
Group comparison

If multiple groups, each group can be backprojected separately and partial factor scores can be used to quantify group differences
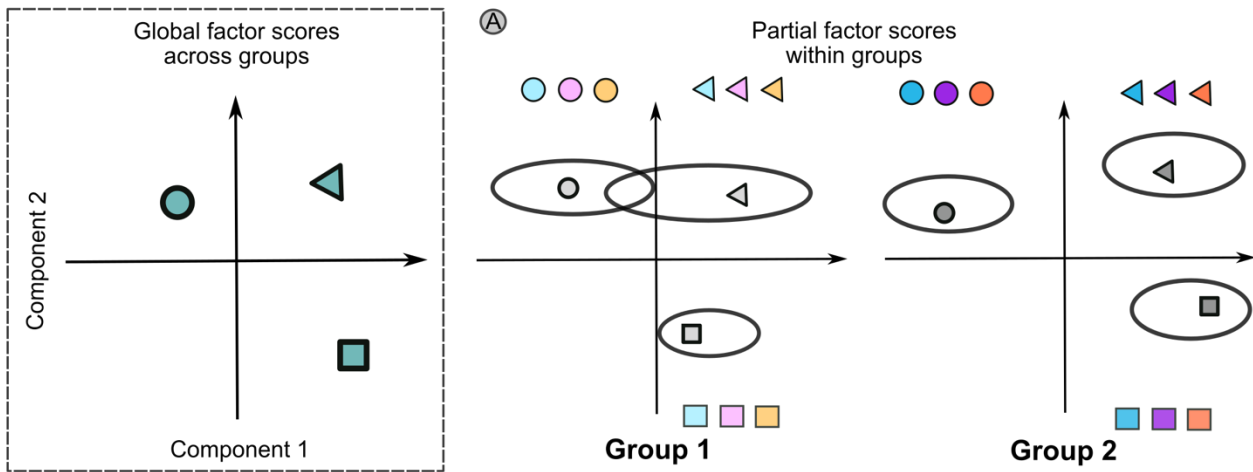
Similarity between observations (across the whole sample or within group) can also be quantified by deriving the area of convex hull
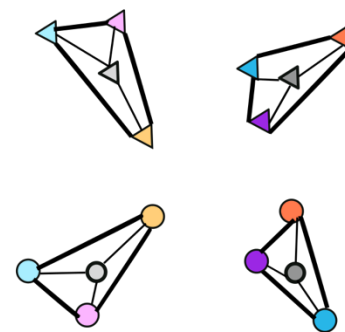
Figure 2. Top panel: examples of applications of covSTATIS in network neuroscience. **Bottom panel:** examples of extractable features from covSTATIS. For instance, **(A)** illustrates how we can extract, from global factor scores, group means of partial factor scores, derive their bootstrap confidence intervals, and use them to interpret group differences in network configurations. **(B)** demonstrates how we can quantify the overall heterogeneity among all partial factor scores via computing the area of the hull. **(C)** shows how such heterogeneity can also be evaluated for different groups separately.

Methods

Notations

A matrix is denoted by a bold, uppercase letter (e.g., $\mathbf{X}$), a vector is denoted by a bold, lowercase letter (e.g., $\mathbf{x}$), and an element of a matrix is denoted by a lowercase italic letter (e.g., x). The cardinal of a set is denoted by an uppercase italic letter (e.g., I). Given I data tables, we used the subscript i to identify individual data tables (e.g., $\mathbf{X}_i$). The boldface capital letter $\mathbf{I}$ denotes the identity matrix. The transpose of a matrix is denoted by the superscript $^\mathrm{T}$ (e.g., $\mathbf{X}^\mathrm{T}$).

The jth column of matrix $\mathbf{X}$ is denoted by $\mathbf{x}_j$, and the value on the kth row and the jth column is denoted by $x_{i,j}$. For an $I \times J$ matrix, the minimum of I and J is the largest possible rank, denoted by L, of $\mathbf{X}$. The trace($\mathbf{X}$) operator gives the sum of the diagonal elements of the square matrix $\mathbf{X}$.

covSTATIS

To generate the compromise space that best represents the common pattern across all data tables (e.g., correlation/covariance matrices), covSTATIS first derives weights from a pairwise similarity matrix, called the $\mathbf{R_V}$ matrix, which quantifies the similarity between data tables via the R_V coefficient. Formally, given two $J \times J$ data tables $\mathbf{X}_i$ and $\mathbf{X}_{i'}$ (e.g., two connectivity matrices with J ROIs from the 2 observations i and i', e.g., participants or tasks), the R_V coefficient between these two matrices is computed as:

$$R_V = \frac{\mathrm{trace}\left(\mathbf{X}_i^\top \mathbf{X}_{i'}\right)}{\sqrt{\mathrm{trace}\left(\mathbf{X}_i^\top \mathbf{X}_i\right)\mathrm{trace}\left(\mathbf{X}_{i'}^\top \mathbf{X}_{i'}\right)}} = \frac{\sum_{j}^{J}\sum_{j'}^{J} x_{j,j',i}\, x_{j,j',i'}}{\sqrt{\left(\sum_{j}^{J}\sum_{j'}^{J} x_{j,j',i}^2\right)\left(\sum_{j}^{J}\sum_{j'}^{J} x_{j,j',i'}^2\right)}}. \tag{1}$$

Akin to a squared correlation coefficient, the R_V coefficient takes values in the interval [0 1]. The R_V coefficients between all matrices are then stored in an $I \times I$ $\mathbf{R_V}$ matrix, denoted by $\mathbf{C}$, where the cell $c_{i,i'}$ stores the value of the R_V coefficient between $\mathbf{X}_i$ and $\mathbf{X}_{i'}$. As $\mathbf{C}$ gives the similarity between data tables, the first component of $\mathbf{C}$ best represents the common pattern across tables, and the first eigenvector of $\mathbf{C}$ ($\mathbf{u}_1$) quantifies how similar each table is to this common pattern. As a result, to build

the compromise space, weights for each data table are derived by the scaled $\mathbf{u}_1$, scaled to sum to 1. Formally, $\mathbf{C}$ undergoes EVD:

$$\mathbf{C} = \mathbf{U\Omega U}^\top \text{ such that } \mathbf{U}^\top \mathbf{U} = \mathbf{I}, \tag{2}$$

where $\mathbf{\Omega}$ is an $R \times R$ diagonal matrix of eigenvalues of $\mathbf{C}$ with R denoting the rank of $\mathbf{C}$, and $\mathbf{U}$ is a $I \times R$ matrix of eigenvectors of $\mathbf{C}$. Next the weights of $\mathbf{X}_i$ (denoted by α_i) are obtained as:

$$\alpha_i = \sqrt{\frac{u_{i,1}}{\sum\limits_{i=1}^{I} u_{i,1}}} = \left(u_{i,1}(\mathbf{1}^\top \mathbf{u}_1)^{-1} \right)^{\frac{1}{2}}, \tag{3}$$

where u_{i1} is the ith value of $\mathbf{u}_1$, which corresponds to $\mathbf{X}_i$. The compromise ($\mathbf{X}_+$) is then computed as the weighted sum of all data matrices, where

$$\mathbf{X}_+ = \sum_{i=1}^{I} \alpha_i \, \mathbf{X}_i, \tag{4}$$

and decomposed by EVD:

$$\mathbf{X}_+ = \mathbf{P\Lambda P}^\top \text{ such that } \mathbf{P}^\top \mathbf{P} = \mathbf{I}, \tag{5}$$

where $\mathbf{\Lambda}$ is an $L \times L$ diagonal matrix of eigenvalues of $\mathbf{X}_+$ with L denoting the rank of $\mathbf{X}_+$, and $\mathbf{P}$ is a $J \times L$ matrix of eigenvectors of $\mathbf{X}_+$. From EVD, the *global factor scores* $\mathbf{F}$ (i.e., factor scores from the compromise) are computed as:

$$\mathbf{F} = \mathbf{X}_+ \mathbf{P\Lambda}^{-\frac{1}{2}} \tag{6}$$

and the *partial factor scores* $\mathbf{F}_i$ (i.e., the factor scores derived from the projection of individual tables onto the compromise) are computed as:

$$\mathbf{F}_i = \mathbf{X}_i \mathbf{P\Lambda}^{-\frac{1}{2}}. \tag{7}$$

It is worth noting that these partial factor scores have a barycentric property, that is their weighted sums equate to the global factor scores:

$$\mathbf{F} = \sum_{i}^{I} \alpha_i \mathbf{F}_i. \tag{8}$$

The optimization problem in covSTATIS

Optimization in covSTATIS is a two-part problem. The first part is akin to the optimization problem of principal component analysis, the second part is the same as the optimization problem of eigenvalue decomposition.

First part

First, weights for each data table are obtained to compute the compromise, such that the similarity between the compromise and all input matrices is maximal. Second, components are computed that best explain the compromise's inertia (i.e., variance in more than 2 dimensions). Formally, the first optimization problem can be written as the following maximization problem:

$$\arg\max_{\boldsymbol{\alpha}} \sum_{i=1}^{I} \left\langle \mathbf{X}_i, \underbrace{\sum_{i'}^{I} \alpha_{i'} \mathbf{X}_{i'}}_{\mathbf{X}_+} \right\rangle^2 \quad \text{with} \quad \boldsymbol{\alpha}^\top \boldsymbol{\alpha} = 1, \tag{9}$$

and the sum of squared scalar products can be developed and simplified:

$$\begin{aligned}
\sum_{i=1}^{I} \langle \mathbf{X}_i, \mathbf{X}_+ \rangle^2 &= \sum_{i=1}^{I} \sum_{i'=1}^{I} \alpha_i \alpha_{i'} \sum_{i''=1}^{I} \text{trace}\left\{ \mathbf{X}_i \mathbf{X}_{i''} \right\} \times \text{trace}\left\{ \mathbf{X}_{i''} \mathbf{X}_{i'} \right\} \\
&= \sum_{i=1}^{I} \sum_{i'=1}^{I} \boldsymbol{\alpha}_i \boldsymbol{\alpha}_{i'} \sum_{i''=1}^{I} c_{i,i''} \times c_{i'',i'} \\
&= \boldsymbol{\alpha}^\top \mathbf{C}^2 \boldsymbol{\alpha}.
\end{aligned} \tag{10}$$

Therefore, the solution of the optimization problem defined by Equation 9 is the first eigenvector of $\mathbf{C}^2$, which is the same as the first eigenvector of $\mathbf{C}$. According to the Perron-Frobenius theorem, the elements of $\boldsymbol{\alpha}$ will all have the same sign (chosen as positive). These elements are then scaled to sum to 1 to ensure that partial factor scores will be barycentric for their respective global factor scores (cf. Equation 8). Note that we ignored the denominator of the R_V in the first line as it is a fixed scalar equal to J^2 and has no effect on the maximization problem.

This optimization problem is similar to the optimization problem of Principal Component Analysis (PCA). In PCA, weights are searched *for each variable* to compute factor scores—which are computed as linear combinations of these variables. In covSTATIS, weights are searched *for each data table* to compute the compromise—the linear combination of these data tables.

Second part

The second optimization problem is equivalent to the optimization problem of an eigen-decomposition. In the eigen-decomposition, for each component, weights (i.e., loadings) of each row/column are searched to compute factor scores ($\mathbf{F}$). Factor scores are linear combinations of the loadings that have the largest possible variance (as evaluated by their associated eigenvalues). This optimization problem can be written as the minimization problem of approximating the sum of squared factor scores to the compromise:

$$\arg\min_{\mathbf{F}} \left\| \mathbf{X}_+ - \mathbf{F}\mathbf{F}^\top \right\|_2^2 \quad \text{such that} \quad \mathbf{F}^\top\mathbf{F} = \mathbf{\Lambda}$$
$$\Leftrightarrow \arg\min_{\mathbf{P}} \left\| \mathbf{X}_+ - \mathbf{P}\mathbf{\Lambda}\mathbf{P}^\top \right\|_2^2 \quad \text{such that} \quad \mathbf{P}^\top\mathbf{P} = \mathbf{I}. \tag{11}$$

Here, $\mathbf{P}$ is the matrix of eigenvectors and $\mathbf{\Lambda}$ is the diagonal matrix of eigenvalues.

The detailed proofs and descriptions of the optimization problems of covSTATIS can be found in the Appendix of [64].

Data availability

Data used in the tutorial are available online (https://osf.io/hnj7s/) and are described in detail in our previous publication[80].

Code availability

The original source code for covSTATIS can be found here: https://cran.r-project.org/web/packages/DistatisR/ and its helper file here: https://cran.r-project.org/web/packages/DistatisR/DistatisR.pdf. All code used to apply covSTATIS in network neuroscience and replicate our tutorial, along with all documentation, can be accessed here: https://giuliabaracc.github.io/covSTATIS_netneuro/pages/tutorial.html. For the tutorial, a downloadable Rmd file can be accessed here: https://github.com/giuliabaracc/covSTATIS_netneuro/blob/main/pages/tutorial.qmd. The following GitHub (https://github.com/giuliabaracc/covSTATIS_netneuro/tree/main) and website (https://giuliabaracc.github.io/covSTATIS_netneuro/) links serve as centralized resources for covSTATIS' applications in network neuroscience.

Funding

CRediT author statement

Giulia Baracchini: Conceptualization, Software, Formal Analysis, Data Curation, Writing – Original Draft, Writing – Review and Editing, Visualization. **Ju-Chi Yu:** Conceptualization, Software, Formal

References

1. Zalesky, A., Fornito, A. & Bullmore, E. On the use of correlation as a measure of network connectivity. *NeuroImage* **60**, 2096–2106 (2012).

2. Evans, A. C. Networks of anatomical covariance. *NeuroImage* **80**, 489–504 (2013).

3. Pagani, M., Bifone, A. & Gozzi, A. Structural covariance networks in the mouse brain. *NeuroImage* **129**, 55–63 (2016).

4. Bassett, D. S. & Sporns, O. Network neuroscience. *Nat Neurosci* **20**, 353–364 (2017).

5. Poldrack, R. A. *et al.* Long-term neural and physiological phenotyping of a single human. *Nat Commun* **6**, 8885 (2015).

6. Gordon, E. M. *et al.* Precision Functional Mapping of Individual Human Brains. *Neuron* **95**, 791-807.e7 (2017).

7. Taylor, J. R. *et al.* The Cambridge Centre for Ageing and Neuroscience (Cam-CAN) data repository: Structural and functional MRI, MEG, and cognitive data from a cross-sectional adult lifespan sample. *NeuroImage* **144**, 262–269 (2017).

8. Bycroft, C. *et al.* The UK Biobank resource with deep phenotyping and genomic data. *Nature* **562**, 203–209 (2018).

9. Royer, J. *et al.* An Open MRI Dataset For Multiscale Neuroscience. *Sci Data* **9**, 569 (2022).

10. Nooner, K. B. *et al.* The NKI-Rockland Sample: A Model for Accelerating the Pace of Discovery Science in Psychiatry. *Front. Neurosci.* **6**, (2012).

11. Pinho, A. L. *et al.* Individual Brain Charting, a high-resolution fMRI dataset for cognitive mapping. *Sci Data* **5**, 180105 (2018).

12. Allen, E. J. *et al.* A massive 7T fMRI dataset to bridge cognitive neuroscience and artificial intelligence. *Nat Neurosci* **25**, 116–126 (2022).

13. Spreng, R. N. *et al.* Neurocognitive aging data release with behavioral, structural and multi-echo functional MRI measures. *Sci Data* **9**, 119 (2022).

14. Hutchison, R. M. *et al.* Dynamic functional connectivity: Promise, issues, and interpretations. *NeuroImage* **80**, 360–378 (2013).

15. Calhoun, V. D., Miller, R., Pearlson, G. & Adalı, T. The Chronnectome: Time-Varying Connectivity Networks as the Next Frontier in fMRI Data Discovery. *Neuron* **84**, 262–274 (2014).

16. Michel, C. M. & Koenig, T. EEG microstates as a tool for studying the temporal dynamics of whole-brain neuronal networks: A review. *NeuroImage* **180**, 577–593 (2018).

17. Lurie, D. J. *et al.* Questions and controversies in the study of time-varying functional connectivity in resting fMRI. *Network Neuroscience* **4**, 30–69 (2020).

18. Betzel, R. F. & Bassett, D. S. Multi-scale brain networks. *NeuroImage* **160**, 73–83 (2017).

19. Suárez, L. E., Markello, R. D., Betzel, R. F. & Misic, B. Linking Structure and Function in Macroscale Brain Networks. *Trends in Cognitive Sciences* S1364661320300267 (2020) doi:10.1016/j.tics.2020.01.008.

20. Finn, E. S. *et al.* Functional connectome fingerprinting: identifying individuals using patterns of brain connectivity. *Nat Neurosci* **18**, 1664–1671 (2015).

21. Zuo, X.-N. *et al.* Human Connectomics across the Life Span. *Trends in Cognitive Sciences* **21**, 32–45 (2017).

22. Braun, U. *et al.* From Maps to Multi-dimensional Network Mechanisms of Mental Disorders. *Neuron* **97**, 14–31 (2018).

23. Tompson, S. H., Falk, E. B., Vettel, J. M. & Bassett, D. S. Network Approaches to Understand Individual Differences in Brain Connectivity: Opportunities for Personality Neuroscience. *Personality Neuroscience* **1**, e5 (2018).

24. Beaty, R. E., Seli, P. & Schacter, D. L. Network neuroscience of creative cognition: mapping cognitive mechanisms and individual differences in the creative brain. *Current Opinion in Behavioral Sciences* **27**, 22–30 (2019).

25. Krendl, A. C. & Betzel, R. F. Social cognitive network neuroscience. *Social Cognitive and Affective Neuroscience* **17**, 510–529 (2022).

26. Ferreira, L. K. & Busatto, G. F. Resting-state functional connectivity in normal brain aging. *Neuroscience & Biobehavioral Reviews* **37**, 384–400 (2013).

27. Stam, C. J. Modern network science of neurological disorders. *Nat Rev Neurosci* **15**, 683–695 (2014).

28. Medaglia, J. D., Lynall, M.-E. & Bassett, D. S. Cognitive Network Neuroscience. *Journal of Cognitive Neuroscience* **27**, 1471–1491 (2015).

29. Fornito, A., Zalesky, A. & Breakspear, M. The connectomics of brain disorders. *Nat Rev Neurosci* **16**, 159–172 (2015).

30. Zhang, J. *et al.* What have we really learned from functional connectivity in clinical populations? *NeuroImage* **242**, 118466 (2021).

31. Noble, S. *et al.* Multisite reliability of MR-based functional connectivity. *NeuroImage* **146**, 959–970 (2017).

32. Zhang, C., Baum, S. A., Adduru, V. R., Biswal, B. B. & Michael, A. M. Test-retest reliability of dynamic functional connectivity in resting state fMRI. *NeuroImage* **183**, 907–918 (2018).

33. Rubinov, M. & Sporns, O. Complex network measures of brain connectivity: Uses and interpretations. *NeuroImage* **52**, 1059–1069 (2010).

34. Smith, S. M. *et al.* A positive-negative mode of population covariation links brain connectivity, demographics and behavior. *Nat Neurosci* **18**, 1565–1567 (2015).

35. Tucker, L. R. Some mathematical notes on three-mode factor analysis. *Psychometrika* **31**, 279–311 (1966).

36. Harshman, R. A. FOUNDATIONS OF THE PARAFAC PROCEDURE: MODELS AND CONDITIONS FOR AN 'EXPLANATORY' MULTIMODAL FACTOR ANALYSIS.

37. Gower, J. C. Generalized procrustes analysis.

38. Loan, C. F. V. The ubiquitous Kronecker product. *Journal of Computational and Applied Mathematics* **123**, 85–100 (2000).

39. Van Deun, K., Smilde, A. K., Van Der Werf, M. J., Kiers, H. A. & Van Mechelen, I. A structured overview of simultaneous component based data integration. *BMC Bioinformatics* **10**, 246 (2009).

40. Tenenhaus, A. & Tenenhaus, M. Regularized Generalized Canonical Correlation Analysis. *Psychometrika* **76**, 257–284 (2011).

41. Wang, B. *et al.* Similarity network fusion for aggregating data types on a genomic scale. *Nat Methods* **11**, 333–337 (2014).

42. Haxby, J. V., Guntupalli, J. S., Nastase, S. A. & Feilong, M. Hyperalignment: Modeling shared information encoded in idiosyncratic cortical topographies. *eLife* **9**, e56601 (2020).

43. Zhou, J. *et al.* Graph neural networks: A review of methods and applications. *AI Open* **1**, 57–81 (2020).

44. Fried, E. I. *et al.* Mental disorders as networks of problems: a review of recent insights. *Soc Psychiatry Psychiatr Epidemiol* **52**, 1–10 (2017).

45. Zhou, T., Thung, K., Zhu, X. & Shen, D. Effective feature learning and fusion of multimodality data using stage-wise deep neural network for dementia diagnosis. *Human Brain Mapping* **40**, 1001–1016 (2019).

46. Azevedo, T. *et al.* A deep graph neural network architecture for modelling spatio-temporal dynamics in resting-state functional MRI data. *Medical Image Analysis* **79**, 102471 (2022).

47. Zhang, X. *et al.* Multi-View Graph Convolutional Network and Its Applications on Neuroimage Analysis for Parkinson's Disease.

48. Sebenius, I., Campbell, A., Morgan, S. E., Bullmore, E. T. & Lio, P. Multimodal Graph Coarsening for Interpretable, MRI-Based Brain Graph Neural Network. in *2021 IEEE 31st International Workshop on Machine Learning for Signal Processing (MLSP)* 1–6 (IEEE, Gold Coast, Australia, 2021). doi:10.1109/MLSP52302.2021.9690626.

49. Casas-Roma, J. *et al.* Applying multilayer analysis to morphological, structural, and functional brain networks to identify relevant dysfunction patterns. *Network Neuroscience* **6**, 916–933 (2022).

50. Markello, R. D. *et al.* Multimodal phenotypic axes of Parkinson's disease. *npj Parkinsons Dis.* **7**, 6 (2021).

51. Margulies, D. S. *et al.* Situating the default-mode network along a principal gradient of macroscale cortical organization. *Proc Natl Acad Sci USA* **113**, 12574–12579 (2016).

52. Tian, Y., Margulies, D. S., Breakspear, M. & Zalesky, A. Topographic organization of the human subcortex unveiled with functional connectivity gradients. *Nat Neurosci* **23**, 1421–1432 (2020).

53. Vos de Wael, R. *et al.* BrainSpace: a toolbox for the analysis of macroscale gradients in neuroimaging and connectomics datasets. *Commun Biol* **3**, 103 (2020).

54. De Domenico, M. Multilayer modeling and analysis of human brain networks. *GigaScience* **6**, (2017).

55. Muldoon, S. F. & Bassett, D. S. Network and Multilayer Network Approaches to Understanding Human Brain Dynamics. *Philos. of Sci.* **83**, 710–720 (2016).

56. Marquand, A. F., Haak, K. V. & Beckmann, C. F. Functional corticostriatal connection topographies predict goal-directed behaviour in humans. *Nat Hum Behav* **1**, 0146 (2017).

57. Huntenburg, J. M. *et al.* A Systematic Relationship Between Functional Connectivity and Intracortical Myelin in the Human Cerebral Cortex. *Cerebral Cortex* **27**, 981–997 (2017).

58. Larivière, S. *et al.* Multiscale Structure–Function Gradients in the Neonatal Connectome. *Cerebral Cortex* **30**, 47–58 (2020).

59. Betzel, R. F. *et al.* The community structure of functional brain networks exhibits scale-specific patterns of inter- and intra-subject variability. *NeuroImage* **202**, 115990 (2019).

60. Paquola, C. *et al.* Microstructural and functional gradients are increasingly dissociated in transmodal cortices. *PLoS Biol* **17**, e3000284 (2019).

61. Royer, J. *et al.* Gradients of brain organization: smooth sailing from methods development to user community.

62. Coifman, R. R. *et al.* Geometric diffusions as a tool for harmonic analysis and structure definition of data: Diffusion maps. *Proceedings of the National Academy of Sciences* **102**, 7426–7431 (2005).

63. Lafon, S. & Lee, A. B. Diffusion maps and coarse-graining: a unified framework for dimensionality reduction, graph partitioning, and data set parameterization. *IEEE Trans. Pattern Anal. Mach. Intell.* **28**, 1393–1403 (2006).

64. Abdi, H., Williams, L. J., Valentin, D. & Bennani-Dosse, M. STATIS and DISTATIS: optimum multitable principal component analysis and three way metric multidimensional scaling. *WIREs Computational Stats* **4**, 124–167 (2012).

65. Abdi, H., Valentin, D., Chollet, S. & Chrea, C. Analyzing assessors and products in sorting tasks: DISTATIS, theory and applications. *Food Quality and Preference* **18**, 627–640 (2007).

66. Abdi, H. RV Coefficient and Congruence Coefficient.

67. Kherif, F. Group analysis in functional neuroimaging: selecting subjects using similarity measures. *NeuroImage* **20**, 2197–2208 (2003).

68. Shinkareva, S. V., Ombao, H. C., Sutton, B. P., Mohanty, A. & Miller, G. A. Classification of functional brain images with a spatio-temporal dissimilarity map. *NeuroImage* **33**, 63–71 (2006).

69. Abdi, H., Dunlop, J. P. & Williams, L. J. How to compute reliability estimates and display confidence and tolerance intervals for pattern classifiers using the Bootstrap and 3-way multidimensional scaling (DISTATIS). *NeuroImage* **45**, 89–95 (2009).

70. Churchill, N. W. *et al.* Optimizing preprocessing and analysis pipelines for single-subject fMRI. I. Standard temporal motion and physiological noise correction methods. *Human Brain Mapping* **33**, 609–627 (2012).

71. Yourganov, G. *et al.* Pattern classification of fMRI data: Applications for analysis of spatially distributed cortical networks. *NeuroImage* **96**, 117–132 (2014).

72. Sha, L. *et al.* The Animacy Continuum in the Human Ventral Vision Pathway. *Journal of Cognitive Neuroscience* **27**, 665–678 (2015).

73. St-Laurent, M., Abdi, H. & Buchsbaum, B. R. Distributed Patterns of Reactivation Predict Vividness of Recollection. *Journal of Cognitive Neuroscience* **27**, 2000–2018 (2015).

74. Connolly, J. *et al.* Identification of Resting State Networks Involved in Executive Function. *Brain Connect* **6**, 365–374 (2016).

75. Mitchell, D. J. & Cusack, R. Semantic and emotional content of imagined representations in human occipitotemporal cortex. *Sci Rep* **6**, 20232 (2016).

76. Rundle, M. M., Coch, D., Connolly, A. C. & Granger, R. H. Dissociating frequency and animacy effects in visual word processing: An fMRI study. *Brain and Language* **183**, 54–63 (2018).

77. Rieck, J. R., Baracchini, G., Nichol, D., Abdi, H. & Grady, C. L. Reconfiguration and dedifferentiation of functional networks during cognitive control across the adult lifespan. *Neurobiology of Aging* **106**, 80–94 (2021).

78. Baracchini, G. *et al. The Biological Role of Local and Global fMRI BOLD Signal Variability in Human Brain Organization*. http://biorxiv.org/lookup/doi/10.1101/2023.10.22.563476 (2023) doi:10.1101/2023.10.22.563476.

79. Escoufier, Y. Le Traitement des variables vectorielles. *Biometrics* **29**, 751 (1973).

80. Rieck, J. R., Baracchini, G., Nichol, D., Abdi, H. & Grady, C. L. Dataset of functional connectivity during cognitive control for an adult lifespan sample. *Data in Brief* **39**, 107573 (2021).